Differential type of phase-locked laser diode interferometer free from external disturbance

Takamasa Suzuki, Osami Sasaki, Katsuhiro Higuchi, and Takeo Maruyama

A phase-locked laser diode interferometer with differential detection to eliminate external disturbance is proposed. In this interferometer, the measurements are implemented at two different points at the same time. The surface profile that contains the disturbance is obtained at the scanned measuring point, and the disturbance is obtained at the fixed measuring point. The exact profile is obtained by subtracting the latter from the former. The limitations and characteristics are examined theoretically. The analytical results agree well with the experimental results. The repeated measurement accuracy is estimated to be ~ 5 nm in this interferometer.

1. Introduction

Although various kinds of interferometer are used in the manufacturing field for the inspection of optical parts or surface profile measurement of the object and so on, one of the disadvantages of a conventional interferometer is its weakness for external disturbance. Recently, many kinds of interferometer that use a laser diode (LD) have been proposed[1-3] that use the tunability of the wavelength of a LD. In such interferometers it is easy to eliminate the external disturbances by means of feedback control[4,5] in which the tunability of the wavelength is also utilized. But it is difficult for a phase-locked laser diode (PLLD) interferometer[6,7] to introduce feedback control for the elimination of disturbance because the tunability of the wavelength has already been used for the implementation of phase locking.[8-10] Another way to eliminate the disturbance is the incorporation of differential detection for the phase term. In such a system, the phase terms must be obtained at the same time. One is obtained at a fixed point and gives the information of the disturbance. The other is obtained by scanning along the surface of the object, and it contains information about the surface profile of the object and the same disturbance such as that detected at the fixed point. Then, the surface profile is obtained by subtracting the former from the latter.

Since the PLLD interferometer incorporates a discrete-time-control system, phase locking is achieved simultaneously at different measuring points in real time with the time-sharing control. That is to say, simultaneous measurement at different points can be achieved.

In this paper we propose a differential type of PLLD interferometer and examine the characteristics and the measurement accuracy. It is shown that the surface profile can be measured with high accuracy even if external disturbance exists.

2. Principle

Phase detections at fixed measuring point p and scanned measuring point x are achieved by PLLD interferometry. The setup of the PLLD interferometer is shown in Fig. 1. The Twyman–Green interferometer is used as an optical system in which the optical path difference between the two arms is $2D_0$. The LD is modulated sinusoidally[11-13] by the modulation current

$$I_m(t) = a \cos \omega_c t. \qquad (1)$$

The dc bias current I_0, modulation current $I_m(t)$, and control currents $I_c(t, p)$ and $I_c(t, x)$ are injected into the LD by the LD modulator LM. $I_c(t, p)$ and $I_c(t, x)$ are obtained for fixed measuring point p and scanned measuring point x, respectively. I_0 determines the central wavelength λ_0 of the LD. The wavelength of the LD is changed by βI_{in}, where β is the modulation efficiency of the LD and I_{in} is the injection current. The interference signals for points p and x are imaged
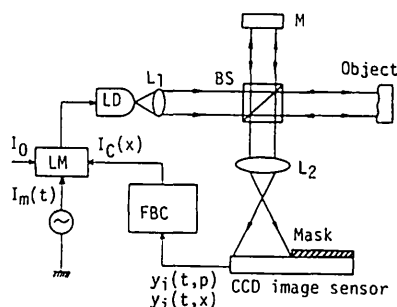
Fig. 1. Experimental setup of a differential-type PLLD interferometer: M, mirror; BS, beam splitter; L's, lenses; LD, laser diode; LM, laser diode modulator; FBC, feedback controller.

onto the charge-coupled device (CCD) image sensor as follows[13]:

$$S(t, x) = S_1 + S_x \cos[z \cos \omega_c t + \alpha(x) + \delta(t)], \quad (2)$$

$$S(t, p) = S_2 + S_p \cos[z \cos \omega_c t + \alpha(p) + \delta(t)], \quad (3)$$

where $z = (4\pi/\lambda_0^2)a\beta D_0$,

$$\alpha(x) + \delta(t) = \{4\pi/[\lambda_0 + \lambda_c(x)]\}[D_0 + D(x) + d(t)], \quad (4)$$

$$\alpha(p) + \delta(t) = \{4\pi/[\lambda_0 + \lambda_c(p)]\}[D_0 + D(p) + d(t)], \quad (5)$$

S_1 and S_2 are the dc components, and S_x and S_p are the amplitudes of the ac components. The surface profile of the object and the external disturbance are represented by $D(x)$ and $d(t)$, respectively. $D(p)$ takes a constant value. $\alpha(x)$ and $\alpha(p)$ are the phase term determined by $D(x)$ and $D(p)$. $\delta(t)$ is also the phase term determined by the disturbance $d(t)$. If the phases represented in Eqs. (4) and (5) are locked to specified value $\alpha(x_0)$ independently, the surface profiles that contain external disturbance are obtained as follows[6,7]:

$$D(x) + d(t) = (D_0/\lambda_0)\beta I_c(t, x), \quad (6)$$

$$D(p) + d(t) = (D_0/\lambda_0)\beta I_c(t, p). \quad (7)$$

By subtracting Eq. (7) from Eq. (6), we can obtain the difference of the surface profile as

$$D(x) - D(p) = (D_0/\lambda_0)\beta[I_c(t, x) - I_c(t, p)]$$

$$= K_c[I_c(t, x) - I_c(t, p)], \quad (8)$$

where $K_c = (D_0/\lambda_0)\beta$. Then the disturbance is removed from the measurement results. Since $D(p)$ is a constant, Eq. (8) represents the exact surface profile of the object.

The PLLD interferometer is equipped with a feedback controller (FBC). In Section 3 we explain the operation of the FBC in detail.

3. Operation of the Feedback Controller

A block diagram of the FBC is shown in Fig. 2. It consists of a feedback signal generator and proportional-integral (PI) controllers. The feedback signal gen-
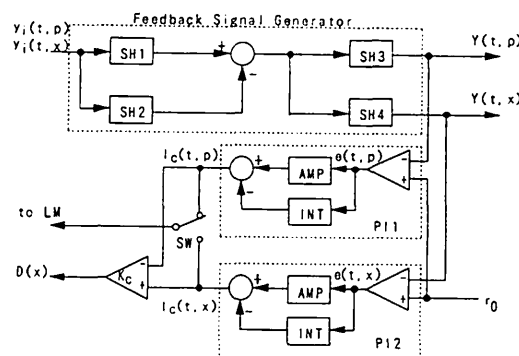

Fig. 2. Block diagram of the FBC: SH's, sample-and-hold circuits; PI's, proportional-integral controllers; SW, switch; AMP, amplifier; int, integrator.

erator uses four sample-and-hold (SH) circuits. The operation of these SH circuits is explained schematically in Fig. 3. The modulation current $I_m(t)$ is shown in Fig. 3(a). The interference signals $S(t, p)$ and $S(t, x)$, which are imaged onto the CCD image sensor, are shown in Fig. 3(b). They are obtained every second period of $I_m(t)$ for the fixed measuring point p and the scanned measuring point x, alternately. The signals y_i show the outputs of the CCD image sensor. Since the output of the CCD image sensor is proportional to the time integration of the incident light, the hatching at y_i means that y_i is an integral value. To simplify the explanation, we take note of the interference signal $S(t, p)$ that was obtained for fixed point p. Since the CCD image sensor is read out synchronously with the modulation current $I_m(t)$, the integral time of $y_1(t, p)$ lies between $-T/4$ and $T/4$. The SH1 samples $y_1(t, p)$ at $t = T/4$ and holds it during the period T as shown in Fig. 3(c), where $T = 2\pi/\omega_c$. In the same way, the SH2 samples and holds $y_2(t, p)$ during the period T as shown in Fig.
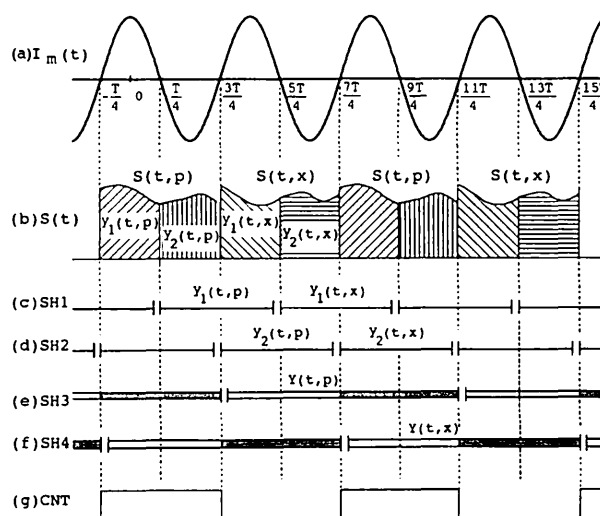

Fig. 3. Generation of the feedback signals: (a) modulation current, (b) interference signals, time chart of the sample-and-hold (SH) circuits, (c) SH1, (d) SH2, (e) SH3, (f) SH4, (g) control (CNT) signal for switch SW.

3(d). The segments under y_i's show the maintenance period of its signal. By subtracting $y_2(t, p)$ from $y_1(t, p)$ at $t = 3T/4$, the feedback signal for fixed point p is obtained as follows[7]:

$$Y(t, p) = y_1(t, p) - y_2(t, p)$$
$$= K_{r1} \sin[\alpha(p) + \delta(t)], \tag{9}$$

where K_{r1} is the amplitude of the feedback signal. The signal $Y(t, p)$ is held between $3T/4$ and $11T/4$ by SH3 as shown in Fig. 3(e). Also the segment under $Y(t, p)$ shows the maintenance period of $Y(t, p)$. The generation process of the feedback signal for measuring point x is the same as that of fixed point p. Then, the feedback signal for measuring point x is obtained as

$$Y(t, x) = y_1(t, x) - y_2(t, x)$$
$$= K_{r2} \sin[\alpha(x) + \delta(t)], \tag{10}$$

where K_{r2} is the amplitude of the feedback signal. $Y(t, x)$ is held by SH4 between $7T/4$ and $15T/4$ as shown in Fig. 3(f). Thus the feedback signals are obtained by overlapping the signals that are then fed into PI controllers as shown in Fig. 2. The PI controllers are the same as those described in Ref. 7. The proportional gain K_p and the integral time T_I in PI controller 1 (PI1) are set to be the same as those of PI controller 2 (PI2). Their output is alternately introduced to the LD through the LM each T period by using the switch SW. The control sequence of SW is shown in Fig. 3(g). The output of PI1 and PI2 is fed to the LM when the control signal CNT is high and low, respectively. Since the feedback signals Y do not change until the next sampling point, the two feedback loops act independently. Consequently, the sampling period T_c of each feedback loop becomes $2T$. The control currents $I_c(t, p)$ and $I_c(t, x)$ are introduced to the differential amplifier whose gain is K_c. Then the exact surface profile can be obtained in real time by Eq. (8).

4. Analysis of the Elimination of Disturbance

Now we discuss analytically the limitation of the elimination of disturbance in our system. Although there are two feedback loops in the system, the block diagram of the control system for the fixed measuring point p is shown in Fig. 4, where variable s represents

a Laplace operation. Since $D(p)$ is a constant, we take note of only the disturbance $d(t)$. The control system for the scanned measuring point x is also the same as that shown in Fig. 4. The transfer functions $G_h(s)$, $G_c(s)$, and $G_s(s)$ are SH circuit, PI controller, and the amplitude of the feedback signal $Y(t, p)$, respectively. They are represented by

$$G_h(s) = [1 - \exp(-T_c s)]/s, \tag{11}$$
$$G_c(s) = K_d[K_p + (1/T_I s)], \tag{12}$$
$$G_s(s) = K_1, \tag{13}$$

where $T_c = 2T$ and $K_1 = K_{r1} = K_{r2}$. The transfer functions $G_a(s)$ and $G_d(s)$ convert the control current $I_c(t, p)$ and the disturbance $d(t)$ to the phases $\alpha_c(t, p)$ and $\delta(t)$, respectively. They are represented by

$$G_a(s) = 4\pi\beta D_0/\lambda_0^2, \tag{14}$$
$$G_d(s) = 4\pi/\lambda_0. \tag{15}$$

We suppose that the disturbance $d(t)$ is sinusoidal and analyze the system by using the z transform. The z transform of the control current $I_c(t, p)$ is given by[7]

$$I_p(z) = E(z)\mathscr{Z}\{G_h(s)G_c(s)\}, \tag{16}$$

where

$$E(z) = -\mathscr{Z}\{G_d(s)G_s(s)D(s)\}/$$
$$[1 + \mathscr{Z}\{G_s(s)G_h(s)G_c(s)G_a(s)\}], \tag{17}$$

and $D(s) = \mathscr{L}\{d(t)\}$. $\mathscr{L}\{f(t)\}$ and $\mathscr{Z}\{f(s)\}$ denote the Laplace transform of $f(t)$ and the z transform of $f(s)$, respectively. If the disturbance $d(t)$ is given by

$$d(t) = v \sin \omega_d(t), \tag{18}$$

the z transform of Eq. (18) is represented by

$$D(z) = \frac{vz \sin \omega_d T_c}{z^2 - 2z \cos \omega_d T_c + 1}. \tag{19}$$

Putting $K_d G_a(s) = K_2$ and $G_d(s) = K_3$, we can represent $I_p(z)$ by

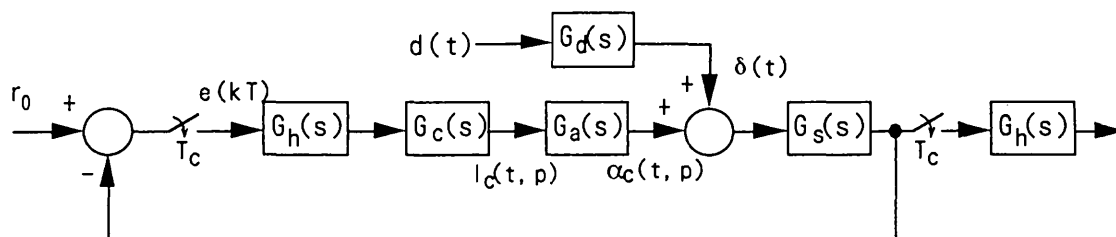$$I_p(z) = -\frac{b_1 z + b_0}{a_1 z + a_0} D(z), \tag{20}$$

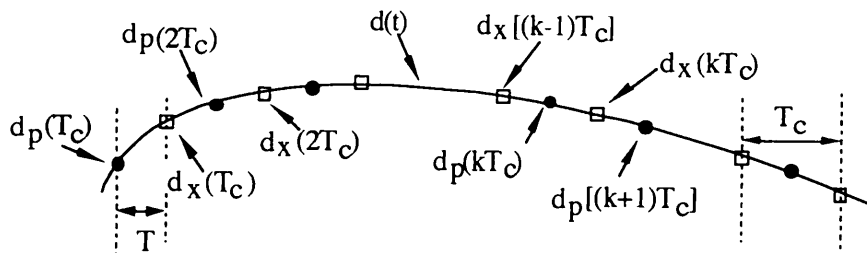Fig. 4. Block diagram of the discrete-time-control system for the scanned measuring point x.

Fig. 5. Series of the measured data lined up along the evolution of the disturbance $d(t)$.

where

$$a_1 = (1 + K_1 K_2 K_P) T_I^2,$$

$$a_0 = T_I \{T_c K_1 K_2 - T_I (1 - K_1 K_2 K_P)\},$$

$$b_1 = K_1 K_3 T_I K_d K_P T_I, \quad b_0 = K_1 K_3 T_I K_d (T_c - K_P T_I).$$

By taking the inverse z transform of $I_p(z)$, we can obtain the series of the control current $I_p(kT_c)$ for the fixed measuring points at each sampling point. The measured error $d_p(kT_c)$ caused by the disturbance $d(t)$ is calculated by

$$d_p(kT_c) = (D_0/\lambda_0)\beta I_p(kT_c). \tag{21}$$

Since the sampling in the feedback loop for point x is delayed just $T_c/2$ compared with that in the feedback loop for point p as shown in Fig. 3, for the analysis of point x it is necessary to use the modified z transform as follows:

$$D(z, 1/2) = \frac{v(z + 1)\sin[\omega_d(T_c/2)]}{z^2 - 2z \cos \omega_d T_c + 1}. \tag{22}$$

The z transform of the control current and the measured error for the scanned measuring point x are given by

$$I_x(z) = -\frac{b_1 z + b_0}{a_1 z + a_0} D(z, 1/2), \tag{23}$$

$$d_x(kT_c) = (D_0/\lambda_0)\beta I_x(kT_c), \tag{24}$$

respectively. Since the series of obtained data is lined up along the evolution of the disturbance $d(t)$ as shown in Fig. 5, by using Eqs. (21) and (24) we calculated the differential error $e_d(kT)$ by

$$e_d[(2n - 1)T] = (d_p(nT_c) - \{d_x[(n - 1)T_c]$$
$$+ d_x(nTc)\}/2),$$

$$e_d(2nT) = (\{d_p(nT_c) + d_p[(n + 1)T_c]\}/2$$
$$- d_x(nTc)), \tag{25}$$

where $n = 1, 2, 3, \ldots$. The characteristic of the elimination of disturbance can be examined by using Eq. (25). If the disturbance can be eliminated completely, $e_d(kT)$ becomes all zero.

5. Experiments

A. Experimental Setup and Control Parameters

The experimental setup is shown in Fig. 1. A 5-mW GaAlAs LD is used as the light source. The central operating wavelength λ_0 is ~ 790 nm, and the modulation efficiency β is 6×10^{-3} nm/mA. The optical path difference $2D_0$ was set to 100 mm. The frequency of phase modulation $1/T$ was 7 kHz, which is limited mainly by the acquisition time of SH1 and SH2. Their acquisition times were 0.5 μs. The measured settling time of the system was ~ 2 ms. The size of the photodetector of the CCD image
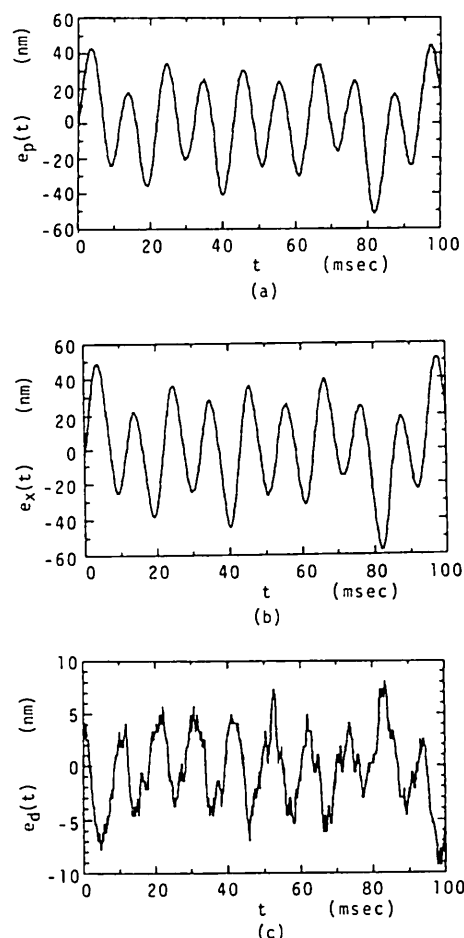

Fig. 6. Disturbances measured at (a) point p, (b) point x, (c) the output of the differential amplifier.

sensor is 9 × 14 μm, and the photodetectors are arranged at intervals of 14 μm. The 50 elements of the photodetectors in the CCD image sensor were used to detect the interference signal. The remaining elements were covered with black paper to eliminate the useless light. The image of the surface of the object was formed onto the CCD image sensor with a magnification of 3.0, so the spatial interval of the measuring points was ~4.7 μm.

The differential gain K_d, the proportional gain K_p, and the integral time T_I of the PI controller were 3.3 × 10^{-5}, 2.0, and 0.1 ms, respectively. The sampling time $T_c = 2T$ was ~0.29 ms.

B. Characteristics of the Elimination of Disturbance

It is considered that the limitation of the elimination of disturbance depends on the amplitude and the frequency of the disturbance. Since the amplitude K_1 of the feedback signal depends on the reflectivity on the surface of the object, it is also expected that the ratio of the reflection at the measuring points affects the limitation of the elimination of disturbance. To clarify these points, we replaced the object by a mirror mounted on the piezoelectric transducer (PZT) in the

experimental setup shown in Fig. 1. The limitation of the elimination of disturbance was examined by vibrating the mirror on the PZT with the sinusoidal signal given in Eq. (18). Both measuring points were fixed. The phase change introduced by the PZT is regarded as the disturbance. The remaining error that could not be eliminated was estimated by calculating its rms value E.

Figures 6(a) and 6(b) show the disturbances measured at points x and p, respectively. Amplitude v and the frequency $f_d = \omega_d/2\pi$ of the disturbance were 50 nm and 100 Hz, respectively. The remaining error or the difference between these disturbances is shown in Fig. 6(c). The sinusoidal vibration was still observed after differential detection. But its amplitude became ~1/10. The rms values E of the remaining error were measured for various conditions as shown in Fig. 7. The plotted data were obtained experimentally. The solid and dashed curves were calculated theoretically for various modulation frequencies by using Eq. (25). Figure 7(a) shows E for various amplitudes of the disturbance. Frequency f_d was 100 Hz. Error E is proportional to amplitude v of the disturbance. Although the error could not be
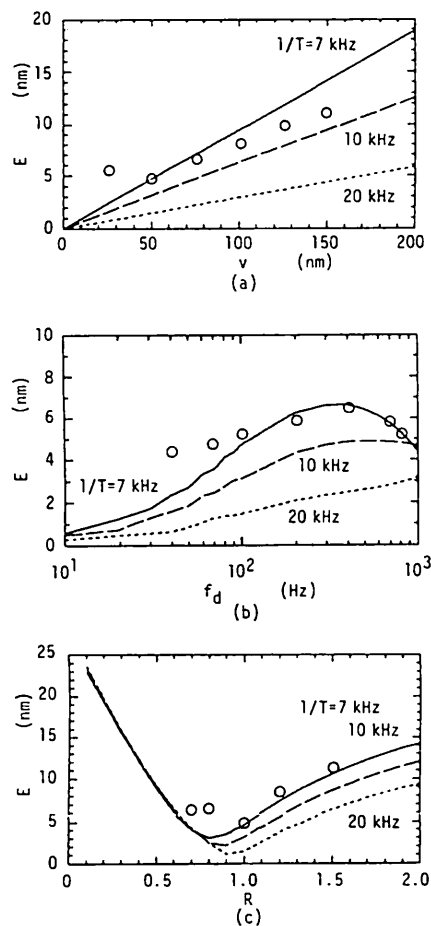

Fig. 7. Dependence of the rms value E of the remaining error on (a) the amplitude of the disturbance, (b) the frequency of the disturbance, (c) the reflective ratio R. O, Experimental plots; solid and dashed curves, theoretical calculations.
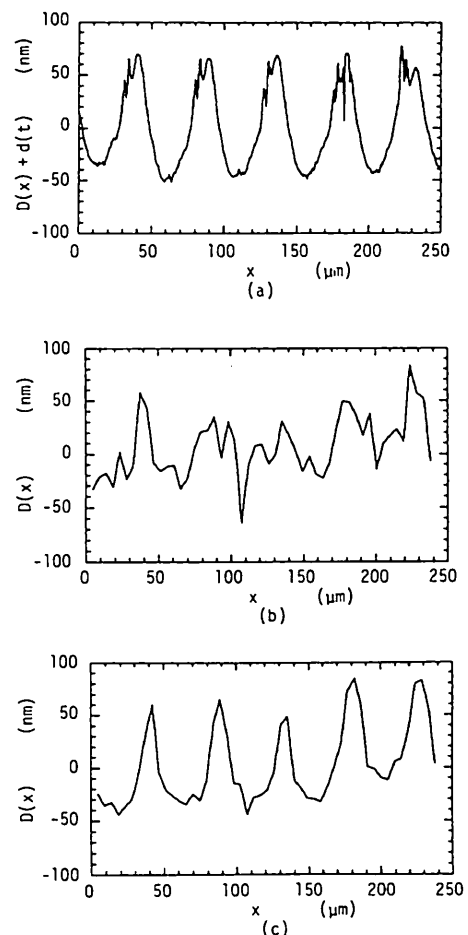
Fig. 8. Surface profiles measured with (a) a Talystep instrument, (b) a conventional PLLD interferometer, (c) differential-type PLLD interferometer.

eliminated completely, the reduced rate for error E gets large according to the increase of modulation frequency. Figure 7(b) shows error E for various f_d's. Amplitude v of the disturbance was 50 nm. The values calculated from Eq. (25) agree well with the measured results. Error E gets large according to the increase of the frequency until $f_d \sim 400$ Hz. But it decreases at the region of $f_d > 400$ Hz. It is thought that the control system cannot follow the disturbance for $f_d > 400$ Hz because the settling time is ~ 2 ms. Error E was measured by changing the gain K_{r1}. The reflective ratio R is defined as

$$R = K_{r1}/K_{r2}, \qquad (26)$$

where K_{r2} is a constant. Amplitude v and the frequency f_d were 50 nm and 100 Hz, respectively. The measured results are shown in Fig. 7(c), where error E does not have a minimum value at $R = 1.0$ because of the discrepancy in sampling time and the detected amplitude of the disturbance. But error E is below ~ 5 nm near $R = 1.0$.

Since the timing of the sampling at the fixed measuring point p is different from that at the scanned measuring point x, it is difficult to eliminate the disturbance completely. But if the interval time between the sampling at point x and that at point p would be reduced by heightening the modulation frequency, the disturbance could be eliminated much more.

C. Measurements of the Surface Profile

We show examples of the measurement of the surface profile. The objects are diamond-turned aluminum disks.

First, the disk whose roughness and cutting pitch were ~ 100 nm and ~ 50 μm, respectively, was measured. Figure 8(a) shows the surface profile measured with a Talystep instrument. It shows a periodic structure determined by the cutting conditions. The surface profile measured at the scanned measuring point x is shown in Fig. 8(b). It is equivalent to the surface profile measured with a conventional PLLD interferometer. Since it contains the external disturbance, the shape is different from that shown in Fig. 8(a). Figure 8(c) shows the surface profile that
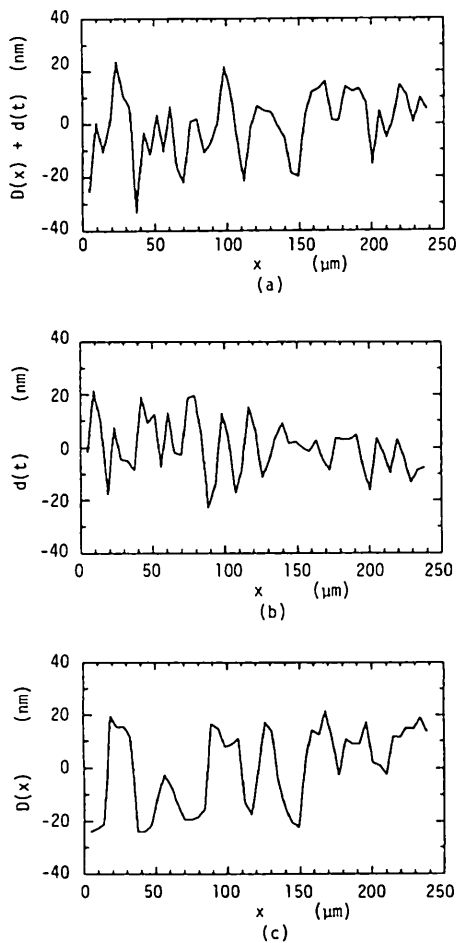

Fig. 9. Experimental results: (a) surface profile that contains the external disturbance measured at the scanned measuring point x, (b) external disturbance measured at the fixed measuring point p, (c) exact surface profile obtained by differential detection.
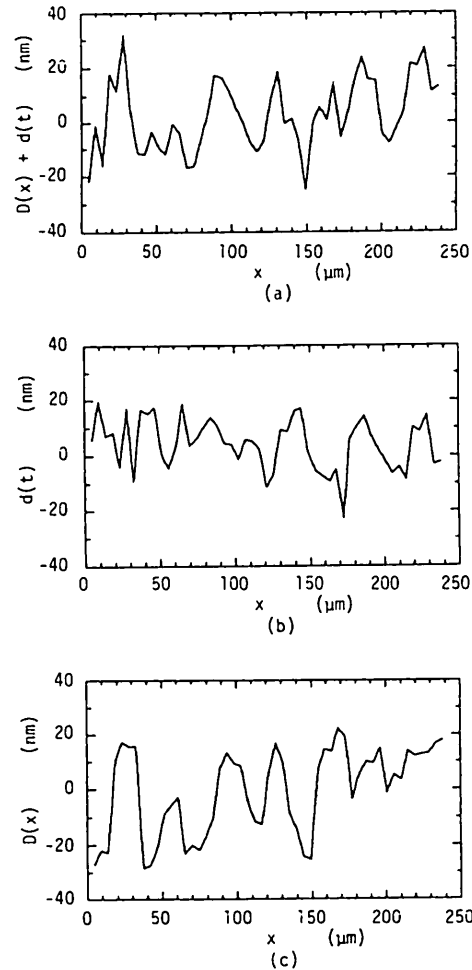

Fig. 10. Experimental results obtained after a few minutes by using the same conditions as in Fig. 9; (a), (b), and (c) correspond to Figs. 9(a), 9(b), and 9(c), respectively.

was measured with a differential-type PLLD interferometer. The measuring points on the surface of the object are different from those in Fig. 8(a). The shapes shown in Figs. 8(a) and 8(c) agree well with each other.

Next, we measured another disk. Its roughness was ~40 nm and the cutting pitch was ~35 μm. The surface profile measured at the scanned measuring point x and the external disturbance measured at the fixed measuring point p are shown in Figs. 9(a) and 9(b), respectively. The surface profile measured with differential detection is shown in Fig. 9(c). It was obtained by subtracting Fig. 9(b) from Fig. 9(a) with a differential amplifier. The periodic structure whose period is ~35 μm is observed in Fig. 9(c). The same disk was measured after a few minutes; the results are shown in Fig. 10. The surface profile that contains the external disturbance is shown in Fig. 10(a). Its shape is different from that in Fig. 9(a) for the sake of the disturbance shown in Fig. 10(b). The rms value of the difference between the two measured surface profiles shown in Figs. 9(a) and 10(a) is ~20 nm. The surface profile measured with the subtraction of the disturbance is shown in Fig. 10(c). The shapes shown in Figs. 9(c) and 10(c) agree well, and the repeated rms measurement accuracy is ~5 nm.

6. Conclusions

A modified-type PLLD interferometer or differential-type PLLD interferometer has been described. It has been shown that the external disturbance can be eliminated with differential detection in this interferometer. The limitation for the elimination of disturbance is examined theoretically by using the z transform. The analytical results agree well with the experimental results. The limitation depends on the amplitude and the frequency of the disturbance and the reflective ratio of the surface of the object. The rms repeated measurement accuracy could be reduced from ~20 to ~5 nm in this interferometer.

Moreover, the rms value E of the remaining error can be reduced much more by heightening the modulation frequency.

References

1. K. Tatsuno and Y. Tsunoda, "Diode laser direct modulation heterodyne interferometer," Appl. Opt. **26**, 37–40 (1987).
2. Y. Ishii, J. Chen, and K. Murata, "Digital phase-measuring interferometry with a tunable laser diode," Opt. Lett. **12**, 233–235 (1987).
3. J. Chen, Y. Ishii, and K. Murata, "Heterodyne interferometry with a frequency-modulated laser diode," Appl. Opt. **27**, 124–128 (1988).
4. T. Yoshino, M. Nara, S. Mnatzakanian, B. S. Lee, and T. C. Strand, "Laser diode feedback interferometer for stabilization and displacement measurements," Appl. Opt. **26**, 892–897 (1987).
5. O. Sasaki, K. Takahashi, and T. Suzuki, "Sinusoidal phase modulating laser diode interferometer with a feedback control system to eliminate external disturbance," Opt. Eng. **29**, 1511–1515 (1990).
6. T. Suzuki, O. Sasaki, and T. Maruyama, "Phase locked laser diode interferometry for surface profile measurement," Appl. Opt. **28**, 4407–4410 (1989).
7. T. Suzuki, O. Sasaki, K. Higuchi, and T. Maruyama, "Phase-locked laser diode interferometer: high-speed feedback control system," Appl. Opt. **30**, 3622–3626 (1991).
8. D. T. Moore, R. P. Murray, and F. B. Neves, "Large aperture ac interferometer for optical testing," Appl. Opt. **17**, 3959–3963 (1978).
9. G. W. Johnson, D. C. Leiner, and D. T. Moore, "Phase-locked interferometry," Opt. Eng. **18**, 46–52 (1979).
10. H. J. Matthews, D. K. Hamilton, and C. J. R. Sheppard, "Surface profiling by phase-locked interferometry," Appl. Opt. **25**, 2372–2374 (1986).
11. O. Sasaki and H. Okazaki, "Sinusoidal phase modulating interferometry for surface profile measurement," Appl. Opt. **25**, 3137–3140 (1986).
12. O. Sasaki and H. Okazaki, "Analysis of measurement accuracy in sinusoidal phase modulating interferometry," Appl. Opt. **25**, 3152–3158 (1986).
13. O. Sasaki, H. Okazaki, and M. Sakai, "Sinusoidal phase modulating interferometer using the integrating-bucket method," Appl. Opt. **26**, 1089–1093 (1987).